Localization and transport of excitation energy in inhomogeneous supramolecular arrays

Vlaming, Sebastiaan Maarten

Chapter 2

Theoretical background

2.1 The Frenkel exciton Hamiltonian

As stated in the introduction, we are interested in the optical and transport properties of strongly coupled molecular systems, such as molecular aggregates. These systems consist of clusters of molecules, such as aggregated dyes or photosynthetic complexes [52, 53], with a large transition dipole moment so that they interact strongly with light. Due to the strong interactions between the molecules, an excitation in such an aggregate will be coherently shared by many molecules in the aggregate. The collective nature of the excited states has important consequences for the optical and transport properties of such systems [22, 54, 55, 61]. While a molecule typically has many possible excited states, one can often focus on one particular excited state that dominates the optical response in a certain energy region. The molecule can then be modeled as an effective two-level system.

The coupling between the molecules in such systems is generally mediated by their transition dipole moments. Labeling the molecules by the index $n = 1, 2..., N$, the Frenkel exciton Hamiltonian is then given by [36, 39, 64]

$$H = \sum_{n=1}^{N} E_n \left|n\right\rangle \left\langle n\right| + \sum_{n,m=1}^{N} J_{nm} \left|n\right\rangle \left\langle m\right|, \tag{2.1.1}$$

where $|n\rangle$ corresponds to a state where molecule n is in the excited state while all others are in their ground state, E_n is its excitation energy, and J_{nm} is the dipole-dipole interaction between molecules n and m. The system is schematically depicted in Fig. 2.1.1. The Frenkel exciton states $|k\rangle$ are the N eigenstates of the Hamiltonian, Eq. 2.1.1, and can be generally written as $|k\rangle = \sum_{n=1}^{N} c_{kn} \left|n\right\rangle$.

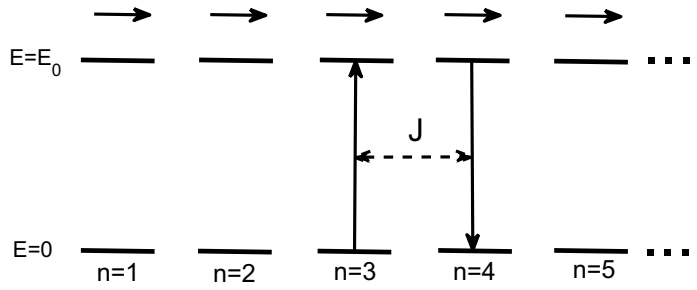

Figure 2.1.1: A schematic depiction of the situation described in the text. We have a chain of two-level molecules, that interact through their transition dipole moments. For simplicity's sake, we have drawn the transition dipole moments equal in magnitude and orientation, and all excitation energies are assumed identical; this is in general not the case.

Assuming point dipoles, the interaction can be written as

$$J_{nm} = \frac{\vec{\mu}_n \cdot \vec{\mu}_m}{|\vec{r}_{nm}|^3} - 3\frac{(\vec{\mu}_n \cdot \vec{r}_{nm})(\vec{\mu}_m \cdot \vec{r}_{nm})}{|\vec{r}_{nm}|^5}, \tag{2.1.2}$$

where $\vec{\mu}_n = \mu_n \hat{e}_n$ is the transition dipole moment vector of molecule n with length μ_n, and $\vec{r}_{nm} \equiv \vec{r}_n - \vec{r}_m$ is the relative position of the molecules n and m.

The point-dipole approximation works well if the distance between molecules is large compared to the spatial extent of the transition dipole moment. If this is not the case, more accurate approaches are necessary. One extension that will be of importance in this thesis is the extended dipole interaction, see Fig. 2.1.2. Here, the point dipole is replaced by two charges $+Q$ and $-Q$ separated by a distance L, such that the magnitude and orientation of the original dipole moment are recovered. The interaction in this scheme is then given by the Coulomb interactions between the four charges,

$$J_{nm} = A\frac{\mu^2}{L^2}\left(\frac{1}{r_{nm}^{++}} - \frac{1}{r_{nm}^{+-}} - \frac{1}{r_{nm}^{-+}} + \frac{1}{r_{nm}^{--}}\right), \tag{2.1.3}$$

with

$$r_{nm}^{\pm\pm} = |\vec{r}_{nm} \pm L(\hat{e}_n - \hat{e}_m)/2|, r_{nm}^{-+} = |\vec{r}_{nm} - L(\hat{e}_n + \hat{e}_m)/2|, r_{nm}^{+-} = |\vec{r}_{nm} + L(\hat{e}_n + \hat{e}_m)/2|, \tag{2.1.4}$$

where $A = 5.04\,\mathrm{cm}^{-1}\mathrm{nm}^3/\mathrm{Debye}^2$ is a numerical constant that allows one to express transition dipole moments in Debye, distances in nm and energies in cm^{-1}. It can be straightforwardly shown that the extended dipole interaction (Eq. 2.1.3) reduces to the point dipole interaction (Eq. 2.1.2) in the limit of short charge separation distances, $L \to 0$.

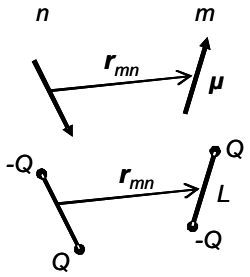

Figure 2.1.2: Point dipoles (left), and the corresponding representation in extended dipoles (right).

The simplest case is given by a homogeneous chain of equidistantly placed molecules with parallel transition dipole moments, i.e. $E_n = E_0$ which in linear optics can be set to zero without loss of generality, $|\vec{r}_{nm}| = |n - m|$ where the lattice parameter has been set to unity, and $\vec{\mu}_n = \vec{\mu}$. Denoting the angle between the transition dipole moment $\vec{\mu}$ and the vector connecting molecules in the chain $\vec{r}_{nm}$ by θ, this gives a dipole-dipole interaction

$$J_{nm} = \frac{\mu^2}{|n-m|^3}\left(1 - 3\cos^2\theta\right). \tag{2.1.5}$$

If the sign of the interaction is negative, i.e. if $\theta < 54.7°$, the system is referred to as a J-aggregate (after Jelley), while a system with a positive interaction is called an H-aggregate (H stands for hypsochromic, denoting a shift to higher energies). The easiest examples of the two are given by transition dipole moments which are parallel ($\theta = 0°$) respectively perpendicular ($\theta = 90°$) to the chain. In this thesis, we will mostly focus on J-aggregates.

An additional possible simplification is to restrict oneself to nearest-neighbor interactions, which in the case of equidistantly placed point dipoles are eight times

stronger than the next strongest interactions, and thus gives a good first indication. It is more accurate to include more interactions, for example the next-nearest-neighbors or even all interactions,and this is also often done in practical numerical calculations. However, the nearest-neighbor approximation has the advantage that it leads to exactly solvable results, which makes it a worthwhile model to study. This leads to the Hamiltonian

$$H = \sum_{n=1}^{N} E_0 \left|n\right\rangle \left\langle n\right| - \sum_{n=1}^{N} J \left|n\right\rangle \left(\left\langle n+1\right| + \left\langle n-1\right|\right), \tag{2.1.6}$$

where the nearest-neighbor interaction $J > 0$ for a J-aggregate. The eigenstates of this Hamiltonian can be found exactly [65, 66], and are

$$\left|k\right\rangle = \left(\frac{2}{N+1}\right)^{1/2} \sum_{n=1}^{N} \sin\left(\frac{\pi k n}{N+1}\right) \left|n\right\rangle. \tag{2.1.7}$$

These states form a one-exciton band of total width $4J$, and have energies

$$E_k = E_0 - 2J \cos\left(\frac{\pi k}{N+1}\right). \tag{2.1.8}$$

If one includes all dipole-dipole interactions, modifications are necessary. In particular, the wave functions and energies will require corrections, with for example an increase in the bandwidth to $E_N - E_1 = 4.207J$. We refer to Refs. [65] and [66] for the details.

2.2 Interaction with light: linear absorption

As was mentioned in Section 2.1, our systems of interest interact strongly with light. In the dipole approximation, the interaction with the light is given by the Hamiltonian term $H_{EM} = -\vec{M} \cdot \vec{E}$, where $\vec{M}$ is the total dipole operator of the aggregate and $\vec{E}$ is the electric field. To calculate the linear absorption spectrum, one typically uses Fermi's golden rule, which follows from a first-order perturbation in the interaction between the system and the electromagnetic field. The total dipole operator of the aggregate is given by

$$\vec{M} = \sum_{n} \vec{\mu}_n \left(b_n^\dagger + b_n\right), \tag{2.2.1}$$

where $b_n^\dagger$ (b_n) creates (annihilates) an excited state on molecule n, and $\vec{\mu}_n$ is its transition dipole moment. It is usually assumed that the systems under consideration are smaller than the wavelength of the incoming light, so that the local

electric field vector $\vec{E}(\vec{r}_n)$ is the same for all molecules in the aggregate. We consider incoming light that is linearly polarized with electric polarization direction $\vec{e}$. The oscillator strength for the transition from the ground state $|g\rangle$ to the exciton state $|k\rangle$ is a measure of how strongly this transition is coupled to the external electromagnetic field. We define it as the square of the corresponding transition dipole operator matrix element,

$$O_k = \left| \langle k | \, \vec{M} \cdot \vec{e} \, | g \rangle \right|^2 = |\vec{\mu}_k \cdot \vec{e}|^2 \,. \tag{2.2.2}$$

The transition dipole moment vector in the exciton basis can straightforwardly be expanded in the site basis,

$$\vec{\mu}_k = \sum_n c_{kn} \vec{\mu}_n. \tag{2.2.3}$$

The spectrum is then given by

$$A(\omega) = \sum_k O_k \delta \left(E_k - \omega \right). \tag{2.2.4}$$

Let us first consider the simplest situation, which is a linear chain of molecules with parallel transition dipole moments. It suffices to consider the case where the polarization vector is parallel to the transition dipole moment vectors; the case for absorption of light of an arbitrary other polarization direction follows trivially. We use the explicit expression Eq. 2.1.7 for the exciton states in a homogeneous chain to obtain their oscillator strengths, leading to

$$O_k = \frac{1 - (-1)^k}{2} \frac{2\mu^2}{N+1} \cot^2 \frac{\pi k}{2(N+1)}. \tag{2.2.5}$$

From the completeness of the set of exciton states, the total oscillator strength can be shown to obey the sum rule $\sum_k O_k = N\mu^2$, i.e. the total oscillator strength of the system is conserved. The absorption spectrum is simply a series of peaks at the exciton energies, with an area that is determined by the oscillator strength of the relevant exciton state. From Eq. 2.2.5, we can straightforwardly see that most of the total oscillator strength, about 81 percent, is collected in the superradiant state $k = 1$. This is a sensible result, as the wave function of the superradiant exciton state has no nodes, so that the contributions from all the molecules interfere constructively. For a J-aggregate, the $k = 1$ state will occur at the bottom of the band at $E_1 \approx -2J$ (for $N \gg 1$). The even states contain no oscillator strength and are therefore dark, while the other odd states carry the remainder of the oscillator strength. For long-range dipole-dipole interactions, these numbers are modified slightly, but qualitatively the behavior remains the same [65]. It can be shown that

also the radiative decay rate of the J-aggregate is superradiantly enhanced with respect to the monomer decay rate [67].

For more complex aggregate geometries, and specifically for the cylindrical aggregates that are studied in this thesis, there are several varieties of the linear absorption spectrum that are of interest. The first is the isotropic linear absorption, where the spectrum is obtained in an isotropic solution of aggregates. Secondly, it is also possible to use an oriented sample by measuring the spectrum in a flow cell. In that case, the aggregates will align to a large extent. One can then measure the absorption for light polarized in the flow direction, but also for light polarized perpendicular to it. This information is often combined into a linear dichroism spectrum (LD), which is the difference in absorption between light polarized in the main direction of the aggregate and light polarized perpendicular to it, $LD(\omega) = A_{||}(\omega) - A_{\perp}(\omega)$.

The structure of the absorption spectrum is the same in all these cases, however, one has to average over the possible relative orientations of the transition dipole moments and the polarization vector. The absorption spectrum is still given by Eq. 2.2.4, where the oscillator strengths now have the form

$$O_k = \left\langle \left| \sum_n c_{kn} \vec{\mu}_n \cdot \vec{e} \right|^2 \right\rangle = \sum_{n,m} c_{kn} c_{km}^* \left\langle (\vec{\mu}_n \cdot \vec{e})(\vec{\mu}_m \cdot \vec{e}) \right\rangle \equiv \sum_{n,m} c_{kn} c_{km}^* O_{nm}, \tag{2.2.6}$$

where the angular brackets $\langle ... \rangle$ denote an orientational average. The factor

$$O_{nm} = \langle (\vec{\mu}_n \cdot \vec{e})(\vec{\mu}_m \cdot \vec{e}) \rangle \tag{2.2.7}$$

is the oscillator strength in the site basis. For an isotropic solution, the completeness of the set of exciton states dictates that the oscillator strengths obey the sum rule $\sum_k O_k = N\mu^2/3$, where the factor 1/3 follows from the isotropy over the three spatial directions [68]. Certain specific geometries allow for further evaluation of the orientational average in Eq. 2.2.6. The LD spectrum has a similar form, although the averaging should in that case be performed over an oriented instead of over an isotropic sample.

2.3 Transport in exciton chains

The analysis presented in the previous sections concerns an isolated aggregate. In reality, such a system is embedded in a medium, and will also have interactions with other aggregates in the environment. To properly describe such a quantum system in contact with an external bath, one needs the density matrix formalism [69–71].

Generally, one can write the total Hamiltonian as

$$H = H_S + H_B + H_{SB}, \tag{2.3.1}$$

where the three terms stand respectively for the system Hamiltonian, the bath Hamiltonian and the Hamiltonian term that describes the system-bath interaction. We assume that the system-bath coupling is small compared to the other parts of the Hamiltonian. The density matrix corresponding to the wave function $|\psi(t)\rangle$ is given by $\rho(t) = |\psi(t)\rangle \langle\psi(t)|$, and evolves in time according to the Liouville-von Neumann equation ($\hbar$ has been set to unity),

$$i\frac{\partial\rho(t)}{\partial t} = [H(t), \rho(t)]. \tag{2.3.2}$$

This is equivalent to the time evolution of the wave function $|\psi(t)\rangle$ as given by the Schrödinger equation. The density matrix elements in a certain basis are commonly divided into populations, which are the diagonal elements $\rho_{ss}(t) = \langle s| \rho(t) |s\rangle$, and coherences, which are the off-diagonal elements $\rho_{s's} = \langle s'| \rho(t) |s\rangle$ with $s' \neq s$. It is useful to work in the interaction picture, where the time evolution induced by the Hamiltonian terms $H_S + H_B$, which are large compared to the system-bath interaction H_{SB}, is explicitly removed from the time evolution of all operators $A(t)$,

$$A_I(t) = e^{i(H_S+H_B)t} A(t) e^{-i(H_S+H_B)t}. \tag{2.3.3}$$

We are only interested in what happens to the system degrees of freedom, and we will thus consider the reduced density matrix $\rho_{SI}(t)$, which is obtained from the density matrix by tracing out the bath degrees of freedom,

$$\rho_{SI}(t) = \mathrm{tr}_B \rho_I(t). \tag{2.3.4}$$

From this point on, we only consider the reduced density operator in the interaction picture, and we will therefore drop the subscript SI from the reduced density operator. We now make two assumptions: (i) we assume that the bath B has so many degrees of freedom that the effect of any interaction with the system dissipates so quickly that the bath remains in equilibrium; (ii) it is assumed that the time correlations between the system-bath interactions at different times decay quickly, i.e. the evolution of the reduced density matrix $\rho(t)$ only depends on its current value, and not on its values in earlier times. These two approximations are known as the Born approximation and the Markov approximation, respectively, and simplify the time evolution of the reduced density matrix considerably. At this stage, the time evolution of the density matrix elements $\rho_{s's}(t)$ can be written as

$$\dot{\rho}_{s's}(t) = \sum_{r'r} R_{s'sr'r} \exp\left[i\left(E_{s'} - E_s - E_{r'} + E_r\right)t\right] \rho_{r'r}(t). \tag{2.3.5}$$

This equation is known as the Redfield equation [70, 72], where the Redfield tensor elements $R_{s's'r'r}$ can be expressed in terms of the time correlation functions of the system-bath interaction operators. In general, couplings still exist between all elements in the density matrix.

To obtain our final result, we require one more approximation. If the exponent in Eq. 2.3.5 oscillates many times during the typical time intervals we are interested in, all the terms in which the argument of the exponent does not vanish can be set to zero; this is referred to as the secular approximation [70, 71]. Assuming irregularly spaced energies, this condition can be fulfilled in two ways. In the case where $s = s'$ and $r = r'$, Eq. 2.3.5 couples populations to each other. The second coupling that survives the secular approximation occurs when $s = r$ and $s' = r'$, corresponding to a decoupled time evolution equation for each individual coherence $\rho_{ss'}$. Thus, the secular approximation leads to a decoupling of the time evolution of the coherences and the populations. The coherences will decay exponentially in time, while the time evolution of the populations is given by

$$\dot{\rho}_{ss}(t) = \sum_{s' \neq s} W_{ss'} \rho_{s's'}(t) - \sum_{s' \neq s} W_{s's} \rho_{ss}(t). \tag{2.3.6}$$

This is the Pauli master equation [73], and can be simply interpreted as a rate equation for the populations. The first term describes all population that enters state s from all other states s', while the second term describes the population that scatters from state s to all other states s'. For a given system-bath coupling term, the scattering rates $W_{ss'}$ can be calculated.

Our model systems consist of exciton chains, which interact with the surroundings. In particular distortions of and vibrations in the host material will modify the interactions of their constituents with the exciton chain, and thus may alter the properties of the molecules forming the exciton chain. These distortions and vibrations correspond to the phonon modes of the bath. In principle, one can also include couplings to vibrations of the aggregate itself by the same methodology. However, since the density of states of the host vibrations is much larger than that of the aggregate vibrations, it is to be expected that coupling to host vibrations is the dominant contribution. [74, 75] In addition, we are mostly interested in the behavior at relatively low temperatures, where coupling to acoustic phonon modes dominates over coupling to optical phonon modes. [74, 75] This is related to the fact that, for the systems we are interested in, acoustic phonon modes typically have energies that are comparable to the exciton level spacings and are thus more easily excited than optical phonons. Coupling to optical phonons has been studied in Refs. [76] and [77]. We take an on-site bilinear coupling term between the

exciton and (acoustic) phonon modes,

$$H_{ex-ph} = \sum_n V_n^q \left|n\right\rangle \left\langle n\right| \left(b_q^\dagger + b_q\right), \tag{2.3.7}$$

where the operators $b_q^\dagger$ (b_q) create (annihilate) a phonon in mode q. We use Fermi's Golden Rule to obtain scattering rates of the form [74, 78, 79]

$$W_{ss'} = W_0 S(|E_{s'} - E_s|) \sum_n |c_{sn}|^2 |c_{s'n}|^2 \left[\Theta(E_s - E_{s'}) n(E_s - E_{s'}) + \right. \tag{2.3.8}$$

$$\left. \Theta(E_{s'} - E_s)\left(1 + n(E_{s'} - E_s)\right)\right],$$

where the Heaviside function $\Theta(x) = 1$ if $x > 0$ and $\Theta(x) = 0$ if $x < 0$, and $n(E) = \left[\exp(E/T) - 1\right]^{-1}$ is the occupation number of the vibrational mode with energy E (the Boltzmann constant has been set to unity). The phonon spectral density $S(E)$ depends on the details of the exciton-phonon coupling term and the phonon density of states, and will not be specified further here. Finally, the factor $\sum_n c_{sn}^2 c_{s'n}^2$ is a probability overlap term between the initial and final states, which dictates that only scatterings between states that are spatially close by can be efficient.

The different terms in Eq. 2.3.8 have a simple interpretation, see also Fig. 2.3.1. If one starts out in an exciton state s, it is only possible to go to a higher energy state s' by absorbing a phonon with the appropriate energy, which should be thermally available; this is the term corresponding to the first Heaviside function. The second Heaviside function corresponds to transitions from a state s to a lower energy state s', and here, two processes are possible. The first term in the second line of Eq. 2.3.8 simply allows for the possibility to emit a phonon that carries away the excess energy $E_s - E_{s'}$, while the second term in the second line of Eq. 2.3.8 requires the prior presence of a phonon, and corresponds to the stimulated emission of phonons with the appropriate energy.

2.4 Localization

As was mentioned in Section 2.3, differences in interactions with the local surroundings lead to variations in the parameters of the Hamiltonian. These variations change in time, and fast dynamical processes in the environment can be treated in the way discussed in Section 2.3. Environmental changes that are slow compared to the exciton processes can be approximated by variations that are constant in time; this is the limit of static disorder. A common way to model disorder is to treat the energies and/or interactions as stochastic variables, described by some

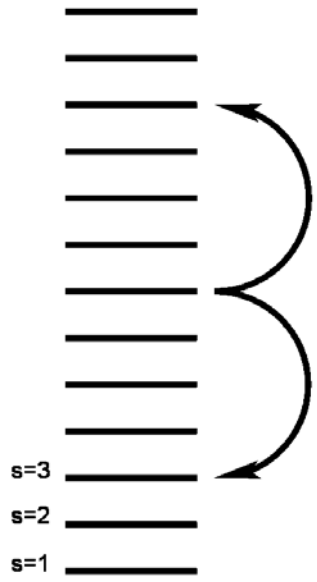

Figure 2.3.1: The exciton band with the possible scatterings. For a scattering event to a higher energy exciton state, absorption of a phonon with the appropriate energy is required. Scattering to a lower energy exciton state can happen spontaneously or can be induced by another phonon; either way, a phonon is emitted to carry away the excess energy.

probability density. In general, the variations in the energies and interactions may be correlated, since they may be due to coupling to the same environmental factors. Such correlated disorder has been studied in, for example, Refs. [80–83]; in this thesis, however, we will limit ourselves to uncorrelated disorder. In principle, both the energies E_n and the interactions J_{nm} may fluctuate. However, the effects of variations in the interactions are in many ways similar to what happens for variations in the energies [65]. For that reason, we will limit ourselves to uncorrelated stochastic distributions for the site energies, which is referred to as uncorrelated diagonal disorder. In certain cases, additional variations in the molecular excitation energies may be present, due to interactions with external fields (Stark effect, for example) or due to an in-built structure where the chromophoric molecules in the aggregate are designed to be different from each other [25, 84–88]. The effect of one such deterministic energy profile, namely a linear variation in excitation energies, is analyzed in Chapter 3 of this thesis.

Philip W. Anderson already showed in the 1950's that disorder can lead to localization of the collective states on segments smaller than the total system size [89]. The typical localization length for the states can be estimated from theoretical arguments; however, except for a few special cases such as Lorentzian disorder (the Lloyd model [90]), few analytical results can be obtained. For a given state $|s\rangle$, we can quantify the typical spatial extent in various ways. A commonly used measure is the participation number (PN) [65, 91, 92],

$$L_s = \left(\sum_{n=1}^{N} c_{sn}^4 \right)^{-1}, \tag{2.4.1}$$

which estimates the number of molecules that coherently share the exciton state $|s\rangle$. It can be easily checked that the PN gives the correct results for a completely localized state ($c_{sn} = \delta_{nn_0}$) or a completely delocalized state ($c_{sn} = \frac{1}{\sqrt{N}}$) on a chain. For higher dimensional aggregates, where we denote the index by a vector $\vec{n} \equiv (n_1, n_2, ...)$, it is more useful to consider the autocorrelation function [93, 94], which is defined as

$$C_s(\vec{n}) = \sum_{\vec{m}} \left| c_{s\vec{m}} c^*_{s,\vec{n}+\vec{m}} \right|, \tag{2.4.2}$$

where the summation over $\vec{m}$ should be taken consistent with the type of boundary conditions we use. For $\vec{n} = \vec{0}$, the autocorrelation function is $C(\vec{0}) = 1$ because of the normalization of the wave functions. For increasing $|\vec{n}|$, the autocorrelation function measures the correlation between the wave functions at different positions and will generally fall off. The length over which the autocorrelation function decays can be interpreted as the localization length, which in general is non-isotropic. The advantage of the autocorrelation function is that it gives information on the direction in which the exciton states are delocalized. Obviously, both measures can also be used to quantify the average localization length for collections of exciton states that share a certain property, such as having an energy within a given energy interval. In that case, one should average Eq. 2.4.1 or Eq. 2.4.2 and normalize with respect to the density of states.

In exciton systems, localization of the exciton states leads to considerable changes of the optical and transport properties. A commonly observed feature is the exchange narrowing effect [65, 80], where collective states that are delocalized over a localization length N^* effectively feel a variation in energy that is a factor $\sqrt{N^*}$ smaller as compared to the monomer. In other words, the exciton absorption peak is narrowed by a factor $\sqrt{N^*}$ as compared to the monomer absorption spectrum. In chapters 4 and 5 of this thesis, it will be shown that the exchange narrowing effect is always present for disorder distributions with a finite second moment, such as Gaussians, but that it is not necessarily the case for more

heavy-tailed distributions (see also Ref. [95]). For example, for Lorentzians or Lévy distributions, the effect may be absent or exchange broadening can occur.

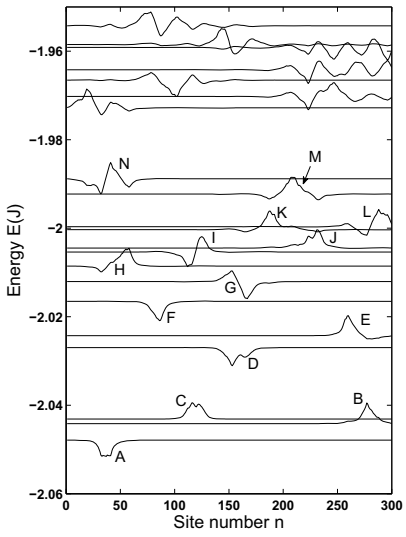

Figure 2.4.1: A typical realization of the wave functions for a chain of length $N = 500$ with Gaussian disorder with standard deviation $\sigma = 0.1J$ and nearest-neighbor interactions. The wave function amplitudes are in arbitrary units and centered around the energy of the corresponding exciton.

Disorder will lead to considerable changes in the exciton wave functions. One such realization for Gaussian disorder is plotted in Fig. 2.4.1; the localization of states is clearly seen to occur. For a homogeneous chain of length N, the solutions are (approximately) given by Eqs. 2.1.7 and 2.1.8. The lowest energy state has no nodes, the second lowest energy state has one node, et cetera. By convention, these states are commonly labeled by s, p, d, f, g, h, and so on, in order of increasing energy. From Fig. 2.4.1, one can see that the exciton wave functions locally resemble those for a homogeneous chain with length N^*, which is the typical localization length for wave functions at the bottom of the band. This is referred to as the hidden structure [66,96]. As an example, we clearly see a triplet structure formed by the states (A, H, N), and doublets formed by the states (C, I), and (D, G). Note that not all localization segments are clearly defined; state (F) is

an s-like state without any companions, and states such as $(K), (L)$ and (M) are delocalized over a number of segments. The states at higher energies are even more delocalized.

The typical energy difference between the exciton states localized on the same segment is comparable to the spread in energy of the local lowest energy states on different localization segments; as a result, the hidden structure is not directly visible in either the linear absorption spectrum or the density of states [66, 96]. The hidden structure is crucial in providing a proper understanding of the exciton transport [97], the Stokes shift [98], and nonlinear spectra [99–101] in such disordered systems, and can thus be unveiled by these methods.

Note that most of the s-like states, i.e. those without nodes, occur at or just below the exciton band edge at $E = -2J$; in Fig. 2.4.1, these are the states $(A), (B), (C), (D), (F)$ and (J). These states collect most of the oscillator strength, and form the so-called Lifshits tail [102]. The fact that the s-like states tend to occur below the exciton band edge directly implies that the exciton absorption shifts to lower energies. The red shift of the exciton absorption spectrum upon increasing disorder is, again, a general result for disorder distributions with a finite second moment. The localization effects are generalized for heavy-tailed distributions in Chapters 4 and 5 of this thesis.

As was shown in Section 2.3, the scattering rate between two exciton states s and s' is proportional to the probability overlap $\sum_n c_{sn}^2 c_{s'n}^2$. Localization will therefore typically reduce the scattering between exciton states on different localization segments. In addition, low energy regions will occur in a chain for a typical disorder realization (see for example the states (a) and (b) in Fig. 2.4.1). Such regions will support exciton states with a low energy, and the local lowest energy states (i.e., the s-like states) on such a localization segment will tend to trap the excitation at low temperatures. If the temperature is sufficiently high, the excitation can scatter to a more delocalized, higher energy state, allowing the energy to escape from the low energy exciton state [74, 97]. These concepts will come back in more detail in Chapter 3 of this thesis.

2.5 The Coherent Potential Approximation

A common way of treating disorder is by repeatedly numerically calculating the relevant quantities for many realizations and averaging the results, see for example Ref. [65]. In this way, the expression for the linear absorption spectrum is a trivial

extension of Eq. 2.2.4,

$$A(\omega) = \left\langle \sum_q O_q \delta(\omega - \omega_q) \right\rangle, \tag{2.5.1}$$

where q labels the eigenstates for a given disorder realization, and the angular brackets $\langle ... \rangle$ denote an average over disorder realizations. While this is perfectly applicable for smaller systems, consisting of several hundreds of molecules, it becomes prohibitively slow for larger systems, such as the cylindrical aggregates in Chapter 6 of this thesis. An elegant alternative is provided by the Coherent Potential Approximation (CPA) [103–105], a mean field method wherein an effective correction factor for the spectra is calculated. In the CPA, we employ the Green's function formalism.

We define the Green's function corresponding to the Hamiltonian H as the operator

$$G(\omega) = (\omega - H + i\eta)^{-1}, \tag{2.5.2}$$

where ω is a complex variable, and η is an infinitesimal positive constant. We can expand the Green's function in terms of the eigenstates $|q\rangle$ (with eigenvalues ω_q) of the Hamiltonian by using the completeness of the eigenstates, $\sum_q |q\rangle \langle q| = 1$,

$$G(\omega) = \sum_q \frac{|q\rangle \langle q|}{\omega - \omega_q + i\eta}. \tag{2.5.3}$$

It can be straightforwardly seen that the Green's function Eq. 2.5.3 has poles on the real axis at the (discrete) eigenenergies; the residues are related to the eigenstates. Similarly, a continuum of solutions leads to a branch cut in the complex plane, where the discontinuity determines the density of states [105].

The linear absorption spectrum Eq. 2.5.1 can simply be written in terms of the Green's function,

$$A(\omega) = -\frac{1}{\pi} \mathrm{Im} \left\langle \sum_q O_q \langle q| G(\omega) |q\rangle \right\rangle, \tag{2.5.4}$$

where Im denotes taking the imaginary part. For an infinitesimally small value of η, this leads to the exact expression in Eq. 2.5.1, while for larger η, we obtain Eq. 2.5.1 convoluted with a Lorentzian lineshape of width η. We can generally expand the oscillator strengths into the site basis (see Eq. 2.2.6),

$$O_q = \sum_{n,m} c_{qn} c_{qm} O_{nm}, \tag{2.5.5}$$

where one should realize that $O_{nm} = \langle(\vec{\mu}_n \cdot \vec{e})(\vec{\mu}_m \cdot \vec{e})\rangle$ is realization independent. In turn this allows us to rewrite Eq. 2.5.4,

$$\left\langle \sum_q O_q \langle q| G(\omega) |q\rangle \right\rangle = \left\langle \sum_{n,m} O_{nm} \langle n| G(\omega) |m\rangle \right\rangle = \sum_{n,m} O_{nm} \langle n| \langle G(\omega)\rangle |m\rangle . \tag{2.5.6}$$

So, if we could calculate the disorder-averaged Green's function (approximately), then we can straightforwardly calculate the spectra in one go, by using the expression

$$A(\omega) = -\frac{1}{\pi} \mathrm{Im} \sum_{n,m} O_{nm} \langle n| \langle G(\omega)\rangle |m\rangle . \tag{2.5.7}$$

In general, $\langle G(\omega)\rangle$ cannot be found exactly. However, it is useful to employ a mean-field approximation scheme. Let us partition the Hamiltonian H in two parts, H_0 and H_1, where H_0 is a part that we can solve and H_1 contains the part on which the eigenstates of H_0 scatter. For notational simplicity, we include the constant $i\eta$ in H_0. The total Green's function $G(\omega)$ can be written as

$$G(\omega) = (\omega - H_0 - H_1)^{-1} = (1 - G_0(\omega)H_1)^{-1} G_0(\omega) = G_0(\omega) + G_0(\omega)H_1G(\omega). \tag{2.5.8}$$

Recursively substituting this back into itself allows us to isolate all the information on the scattering by H_1 into the so-called T-matrix $T(\omega)$,

$$G(\omega) = G_0(\omega) + G_0(\omega)H_1G_0(\omega) + G_0(\omega)H_1G_0(\omega)H_1G_0(\omega) + ... = \tag{2.5.9}$$
$$G_0(\omega) + G_0(\omega)T(\omega)G_0(\omega).$$

Since H_0 is realization independent, the disorder-averaged Green's function is

$$\langle G(\omega)\rangle = G_0(\omega) + G_0(\omega) \langle T(\omega)\rangle G_0(\omega). \tag{2.5.10}$$

The scattering matrix corresponding to a single impurity at site m, having an energy difference E'_m with respect to its surroundings, is given by [105]

$$t_m = \frac{E'_m}{1 - E'_m G_0(m,m)}, \tag{2.5.11}$$

where

$$G_0(m,m) = \langle m|G_0(\omega)|m\rangle = \sum_q \frac{|c_{qm}|^2}{\omega - \omega_q + i\eta}. \tag{2.5.12}$$

Generally, the total scattering matrix T depends on the combinations $\{t_m\}$ of scattering events on individual sites m in some very complicated way,

$$T = f(\{t_m\}). \tag{2.5.13}$$

We now introduce the Average T-matrix Approximation (ATA), where it is assumed that the disorder average of products of individual scatterings is equal to the products of the disorder averaged individual scatterings, $\langle t_m t_n \rangle = \langle t_m \rangle \langle t_n \rangle$ and so on for higher order products. Since we can now decompose all products in T, we have

$$\langle T \rangle = f\left(\{\langle t_m \rangle\}\right). \tag{2.5.14}$$

The complex self-energy $\Sigma(\omega)$ is now defined in such a way that it reproduces the average scattering,

$$\langle t_m \rangle = \frac{\Sigma(\omega)}{1 - \Sigma(\omega) G_0(m,m)}. \tag{2.5.15}$$

We can easily solve for the self-energy,

$$\Sigma(\omega) = \frac{\langle t_m \rangle}{1 + \langle t_m \rangle G_0(m,m)}. \tag{2.5.16}$$

In the ATA, the effect of the scattering part of the Hamiltonian H_1 is now replaced by its average, the self-energy, so that the effective Hamiltonian is $H_{\text{eff}} = H_0 + \Sigma(\omega)$. For the averaged Green's function, this yields

$$\langle G(\omega) \rangle = \frac{1}{\omega - H_0 - \Sigma(\omega) + i\eta}. \tag{2.5.17}$$

Thus, the self-energy $\Sigma(\omega)$ provides a frequency dependent, complex correction factor for the spectrum to account for the effect of the Hamiltonian contribution H_1.

The ATA is easy to use, but it is in many cases not a very accurate approximation; the disorder averages of higher order products of t_m do in general not decompose. The method can be improved upon, though. Again, we introduce a correction factor $\Sigma(\omega)$ that on average accounts for all effects of scattering on H_1, but we partition the Hamiltonian $H = H_0 + H_1 \equiv H_{\text{eff}} + H_1'$ in a slightly different way,

$$H_{\text{eff}} = H_0 + \Sigma(\omega) \; ; \quad H_1' = H_1 - \Sigma(\omega). \tag{2.5.18}$$

The same procedure as in the ATA is followed. The scattering on a site m due to H_1' is given by

$$t_m' = \frac{E_m' - \Sigma(\omega)}{1 - (E_m' - \Sigma(\omega)) G_e(m,m)}, \tag{2.5.19}$$

where G_e is the Green's function corresponding to the effective Hamiltonian H_{eff}. We now make the Coherent Potential Approximation (CPA), which is given by

$$\langle T' \rangle = f\left(\{\langle t_m' \rangle\}\right). \tag{2.5.20}$$

By definition, the scattering on H_1 is on average given by the self-energy $\Sigma(\omega)$, so that

$$G_e = \langle G \rangle \Rightarrow \langle T' \rangle = 0 \Rightarrow \langle t'_m \rangle = 0. \tag{2.5.21}$$

The final equation provides a self-consistent definition of $\Sigma(\omega)$, i.e. it should be chosen such that it corresponds to the effect of all scatterings, and should therefore on average not be affected by any local scattering anymore,

$$\left\langle \frac{E'_m - \Sigma(\omega)}{1 - (E'_m - \Sigma(\omega))G_e(m,m)} \right\rangle = 0. \tag{2.5.22}$$

Note that we have not specified the form of H_1; in fact, the CPA can be used for different Hamiltonian contributions. Let us first consider the case of uncorrelated static disorder. In that case, the disorder average $\langle ... \rangle$ means $\int dE'_m P(E'_m)...$, and the self-consistency condition Eq. 2.5.22 can be straightforwardly rewritten to the iterative form

$$\Sigma(\omega) = \left[\int dx \frac{xP(x)}{1 - (x - \Sigma(\omega))G_e(m,m)} \right] \left[\int dx \frac{P(x)}{1 - (x - \Sigma(\omega))G_e(m,m)} \right]^{-1}. \tag{2.5.23}$$

This provides a practical, rapidly converging scheme to calculate $\Sigma(\omega)$. For each frequency ω, one can start with $\Sigma(\omega) = 0$, proceed with calculating the Green's function, perform the integrals, and iterate the resulting self-energy. For certain choices of the disorder distribution $P(x)$, the integrals in Eq. 2.5.23 can be done exactly, such as box disorder, Lorentzian disorder and dichotomic disorder (i.e., a distribution where the energy can take on two different values); for a Gaussian distribution, one needs to perform the integrals numerically. Note that expressions such as Eqs. 2.5.22 and 2.5.23 are local in frequency, i.e., the self-energies at different frequencies do not mix, so that the self-energy at each frequency can be calculated separately.

It should be noted that the expressions for $\Sigma(\omega)$ still contain a site dependence through the diagonal elements of the Green's function $G_e(m,m)$, while the self-energy is not site dependent. Originally, the CPA was developed for systems with periodic boundary conditions, in which case the Green's function becomes independent of the site m. For finite size systems, we can also remove the site dependence by simply replacing $G_e(m,m)$ by the average over the diagonal elements of the Green's function [94],

$$G_e(m,m) \approx \frac{1}{N} \sum_n G_e(n,n). \tag{2.5.24}$$

Once the self-energy has been determined, the calculation of the spectra is straightforward, as it merely requires the solution of the homogeneous system H_0. Within

the CPA, the Green's function is thus diagonal in the homogeneous basis $|k\rangle$, and the expression for the spectra, Eq. 2.5.7, can be rewritten as

$$A(\omega) = -\frac{1}{\pi}\sum_k O_k \langle k| \langle G(\omega)\rangle |k\rangle = -\frac{1}{\pi}\sum_k O_k \frac{1}{\omega - E_k - \Sigma(\omega) + i\eta}. \qquad (2.5.25)$$

In this thesis, we only employ the CPA to account for the effects of uncorrelated diagonal disorder. However, the method can also be used to treat, for example, dynamical (time-dependent) disorder [106] or exciton-phonon coupling [107–110]; this is usually referred to as the Dynamical Coherent Potential Approximation (DCPA). The DCPA is more complicated to use in practice, though, because the expressions for the self-energy $\Sigma(\omega)$ become nonlocal in frequency. For some simple models, such as coupling to an Einstein phonon system at temperature $T = 0$, the DCPA is still workable. However, if one wants to treat more realistic models including nontrivial phonon dispersion relations and higher temperatures, the DCPA becomes rather unwieldy. To complicate matters even further, adding both static disorder and an exciton-phonon coupling term leads to mixed self-energies that cannot be properly separated.

2.6 Cylindrical aggregates

The geometry of a cylindrical aggregate is most easily described by a stack of rings, as shown in Fig. 2.6.1. Here, each molecule is identified by two indices n_1 and n_2, which label the ring and the position within the ring, which can be conveniently combined into a vectorial index $\vec{n} = (n_1, n_2)$. The total number of rings is N_1 and the number of molecules on a ring is N_2. The inter-ring distance is given by h, the rings have radius R and neighboring rings are rotated over an angle γ. The two angles α and β define the orientation of the transition dipole moment with respect to the cylinder. In particular, β denotes the angle between the transition dipole moment and the cylinder axis, while α is the angle between the projection of the transition dipole moment on the ring plane and the tangent of the ring. The position vector $\vec{r}_{\vec{n}}$ and the transition dipole moment $\vec{\mu}_{\vec{n}}$ can be directly expressed in terms of the above parameters [68]. The Hamiltonian is simply given by Eq. 2.1.1 with either point-dipole interactions, as in Eq. 2.1.2, or extended dipole interactions, given by Eq. 2.1.3,

$$H = \sum_{\vec{n}} E_{\vec{n}} b^\dagger_{\vec{n}} b_{\vec{n}} + \sum_{\vec{n},\vec{m}} J_{\vec{n},\vec{m}} b^\dagger_{\vec{n}} b_{\vec{m}}. \qquad (2.6.1)$$

When one considers a homogeneous cylinder, $E_{\vec{n}} = E_0$, it is possible to exploit the cylindrical symmetry of the aggregate. We explicitly use a Bloch form in the

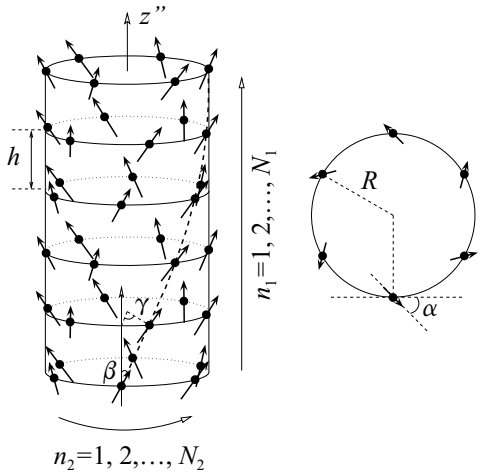

Figure 2.6.1: The cylindrical stack-of-rings geometry. This picture is taken from Ref. [68].

ring direction n_2, and define the transformed creation operator as

$$c^\dagger_{n_1 k_2} = \frac{1}{\sqrt{N_2}} \sum_{n_2} e^{i k_2 \phi_2 n_2} b_{\vec{n}}, \tag{2.6.2}$$

with $\phi_2 = 2\pi/N_2$, and its conjugate expression for the annihilation operator. In this way, the Hamiltonian 2.6.1 decouples into a set of simpler one-dimensional Hamiltonians,

$$H = \sum_{k_2} H(k_2) = \sum_{k_2} \left(\sum_{n_1} E_0 c^\dagger_{n_1 k_2} c_{n_1 k_2} + \sum_{n_1 m_1} J(n_1 - m_1; k_2) c^\dagger_{n_1 k_2} c_{m_1 k_2} \right), \tag{2.6.3}$$

where we have defined $J(n_1; k_2) = \sum_{n_2} e^{-i k_2 \phi_2 n_2} J(n)$, i.e. the interaction between two rings in the Bloch state k_2, a distance $n_1 h$ apart. It can be straightforwardly shown that it suffices to only consider the case $k_2 \geq 0$, as $H(k_2)$ and $H(-k_2)$ have the same eigenvalues while the corresponding eigenvectors are each other's complex conjugate, so that the solutions for $k_2 < 0$ can straightforwardly be found from the solutions with $k_2 \geq 0$ [68].

As was shown in Sec. 2.2, the linear absorption spectrum is given by

$$A(\omega) = \sum_{\vec{k}} O_{\vec{k}} \delta(\omega - E_{\vec{k}}), \tag{2.6.4}$$

with the oscillator strengths

$$O_{\vec{k}} = \sum_{\vec{n},\vec{m}} c_{\vec{k}\vec{n}} c^*_{\vec{k}\vec{m}} \left\langle (\vec{\mu}_{\vec{n}} \cdot \vec{e})(\vec{\mu}_{\vec{m}} \cdot \vec{e}) \right\rangle, \tag{2.6.5}$$

where the angular brackets $\langle ... \rangle$ denote an orientational average. For the cylindrical geometry mentioned above, the orientational average can be straightforwardly evaluated. For an isotropic solution, this yields

$$\left\langle (\vec{\mu}_{\vec{n}} \cdot \vec{e})(\vec{\mu}_{\vec{m}} \cdot \vec{e}) \right\rangle = \frac{1}{3}\mu^2 \left(\sin^2\beta \cos\left[(n_2 - m_2)\phi_2 + (n_1 - m_1)\gamma\right] + \cos^2\beta \right). \tag{2.6.6}$$

Substitution into Eq. 2.2.6, and using the Bloch form in the ring direction for the exciton coefficients, $c_{\vec{k}\vec{n}} = \frac{1}{\sqrt{N_2}} e^{ik_2\phi_2 n_2} \tilde{c}_{k_1}(n_1; k_2)$, leads to the conclusion that only the exciton bands with $k_2 = 0$ and $k_2 = \pm 1$ carry oscillator strength. Explicitly, the oscillator strengths are given by

$$O_{\vec{k}} = \frac{N_2 \mu^2 \cos^2\beta}{3} \delta_{k_2,0} \left| \sum_{n_1} \tilde{c}_{k_1}(n_1; 0) \right|^2 + \frac{N_2 \mu^2 \cos^2\beta}{6} \left(\delta_{k_2,1} \left| \sum_{n_1} \tilde{c}_{k_1}(n_1; 1) e^{-in_1\gamma} \right|^2 \right. \tag{2.6.7}$$

$$\left. + \delta_{k_2,-1} \left| \sum_{n_1} \tilde{c}_{k_1}(n_1; -1) e^{in_1\gamma} \right|^2 \right).$$

That the $k_2 = 0$ and $k_2 = \pm 1$ transitions carry oscillator strength can also be convincingly shown by geometrical arguments. For $k_2 = 0$ transitions, all molecules in a ring have the same prefactor $c_{\vec{k}\vec{n}}$, and the exciton transition dipole moment is simply the weighted sum of the molecular transition dipole moments (cf. Eq. 2.2.3). From Fig. 2.6.1, it can be directly seen that the components in the ring plane cancel, while the components in the cylinder axis direction add. The $k_2 = 0$ transitions are thus polarized in the direction of the cylinder axis. For the $k_2 = \pm 1$ transitions, molecules on opposite sides of the ring have coefficients that differ by a phase factor of -1. As a result, now the ring plane components of the transition dipole moments add, while the axis direction components cancel. Thus, the $k_2 = \pm 1$ transitions are polarized perpendicular to the cylinder axis.

As is common for one-dimensional exciton systems, the optical response of each exciton band $H(k_2)$ is dominated by a small number of superradiant contributions [68, 111]. In fact, for sufficiently long cylinders, one can also use periodic

boundary conditions in the axis direction. In that case, the only remaining contributions to the absorption spectra come from the states with $\vec{k} = (0, 0)$ and $\vec{k} = \pm(k_h, 1)$, with $k_h \equiv \gamma/\phi_1$. Since the $k_2 = \pm 1$ bands are degenerate, one sees that absorption spectrum for a cylindrical aggregate is dominated by two peaks: one from an axially polarized transition with $k_2 = 0$, and one from two degenerate transitions with $k_2 = \pm 1$ which are polarized perpendicular to the cylinder axis.

The calculation for the linear dichroism goes in a completely analogous way; the only difference is that the orientational average is performed in a different way, leading to different numerical prefactors [68]. This yields

$$LD(\omega) = A_{||}(\omega) - A_{\perp}(\omega) = \sum_{\vec{k}} L_{\vec{k}} \delta(\omega - E_{\vec{k}}), \tag{2.6.8}$$

with

$$L_{\vec{k}} = N_2 \mu^2 \cos^2\beta \delta_{k_2,0} \left| \sum_{n_1} \tilde{c}_{k_1}(n_1; 0) \right|^2 - \frac{N_2 \mu^2 \cos^2\beta}{4} \left(\delta_{k_2,1} \left| \sum_{n_1} \tilde{c}_{k_1}(n_1; 1) e^{-i n_1 \gamma} \right|^2 \right. \\ \left. + \delta_{k_2,-1} \left| \sum_{n_1} \tilde{c}_{k_1}(n_1; -1) e^{i n_1 \gamma} \right|^2 \right). \tag{2.6.9}$$

It is useful to note that, in agreement with the geometrical arguments presented above, the LD gives contributions of a positive sign for the axially polarized $k_2 = 0$ transitions, and negative contributions for the ring plane polarized $k_2 = \pm 1$ transitions.

The selection rules obtained here are absolute only for homogeneous cylindrical aggregates. For disordered aggregates, the Bloch states are no longer exact solutions, and exciton states that are localized on segments of the cylinder will occur. As a result, the selection rules will be broken to an extent, and the $k_2 = 0$ and $k_2 = \pm 1$ states will mix. The disorder may be any deviation from the perfectly symmetric homogeneous cylinder, such as energetic disorder [61, 94], deformation of the cylinder [61–63], or disorder in the orientations of the transition dipole moments [62, 63].